Journal of
Biomedical Optics

SPIEDigitalLibrary.org/jbo

Lipidots: competitive organic alternative to quantum dots for *in vivo* fluorescence imaging

Julien Gravier
Fabrice P. Navarro
Thomas Delmas
Frédérique Mittler
Anne-Claude Couffin
Françoise Vinet
Isabelle Texier

SPIE

Journal of Biomedical Optics 16(9), 096013 (September 2011)

Lipidots: competitive organic alternative to quantum dots for *in vivo* fluorescence imaging

Julien Gravier, Fabrice P. Navarro, Thomas Delmas, Frédérique Mittler, Anne-Claude Couffin,
Françoise Vinet, and Isabelle Texier
CEA Grenoble, LETI-DTBS, MINATEC Campus, Grenoble, 38054 France

Abstract. The use of fluorescent nanostructures can bring several benefits on the signal to background ratio for *in vitro* microscopy, *in vivo* small animal imaging, and image-guided surgery. Fluorescent quantum dots (QDs) display outstanding optical properties, with high brightness and low photobleaching rate. However, because of their toxic element core composition and their potential long term retention in reticulo-endothelial organs such as liver, their *in vivo* human applications seem compromised. The development of new dye-loaded (DiO, DiI, DiD, DiR, and Indocyanine Green (ICG)) lipid nanoparticles for fluorescence imaging (lipidots) is described here. Lipidot optical properties quantitatively compete with those of commercial QDs (QTracker®705). Multichannel *in vivo* imaging of lymph nodes in mice is demonstrated for doses as low as 2 pmols of particles. Along with their optical properties, fluorescent lipidots display very low cytotoxicity ($IC_{50} > 75$ nM), which make them suitable tools for *in vitro*, and especially *in vivo*, fluorescence imaging applications. *© 2011 Society of Photo-Optical Instrumentation Engineers (SPIE).* [DOI: 10.1117/1.3625405]

Keywords: fluorescence imaging; lymph node mapping; lipid nanoparticles; organic dyes; quantum dots.

Paper 11187PR received Apr. 13, 2011; revised manuscript received Jul. 8, 2011; accepted for publication Jul. 22, 2011; published online Sep. 14, 2011.

1 Introduction

With the development of a large choice of set-ups dedicated to routine measurements in rodents, the use of *in vivo* fluorescence imaging has been intensified in the field of drug discovery during the last 5 years.[1,2] Human clinical uses for diagnostic and image-guided surgery also emerge as an intensive field of research.[3–14] Special attention has been focused on lymph node imaging. In oncology, precious insights about the possibility of metastatic progression can be obtained by removing the sentinel lymph node, first lymph node draining the tumor, and analyzing it to determine the presence or absence of malignant cells.[3] The current clinical procedure, relying on the injection of a radioactive tracer, exposes the patient and caregivers to ionizing radiations and might be difficult to implement in a surgery room. Real-time near-infrared (NIR) fluorescence imaging for lymph node detection seems to be a hopeful approach.[5–9,11–14] Thanks to their *in vivo* stability and outstanding optical properties, quantum dots (QDs)[15,16] have been considered for this application. It has been shown that QDs can quickly stain the lymph nodes due to their size range (5 to 25 nm). Smaller molecules travel beyond the lymph nodes, whereas larger particles require a long time (24 h) to reach them.[3,14,17,18] However, QDs with a diameter larger than 5 nm are not metabolized and poorly excreted from the body through renal filtration.[19] Furthermore, due to their heavy metal content, they might present a high toxicological risk rendering them dangerous and not adapted for human use. This explains the need for organic alternatives in clinical studies and applications.[14] It has already been reported that lipid-based nanocarriers, such as liposomes and nanoemulsions, likely due to their lipid nature, are rather lymphotropic.[20] For instance, Akers et al. proposed lymph node mapping using dye-loaded perfluorocarbon nanoemulsions and fluorescence or photoacoustic imaging.[17] In another strategy, octanethiol coated gold nanoparticles, photoacoustic agent contrasts, were encapsulated in lipid nanoemulsions.[18]

Among the wide range of nanocarriers, lipid nanoemulsions present several advantages for the design of biocompatible fluorescent probes: i. they can be designed from already approved human-use surfactants and inexpensive natural ingredients, such as glycerides and phospholipids (limitations of toxicity risks); ii. they can be manufactured by solvent-free up-scalable techniques; iii. their lipid core constitutes an ideal reservoir for the high loading of hydrophobic molecules, such as organic fluorophores, whose structure generally displays aromatic moieties with low water solubility; iv. their lipid core provides the encapsulated dye with an apolar and very viscous local environment promoting a high fluorescence quantum yield.[21] The potential difficulty that is often encountered with lipid nanoemulsions is their lack of long term stability, since they are not thermodynamically stable. We recently demonstrated that long-term stability of lipid droplets can be easily achieved using entropic stabilization through mixture contribution of water insoluble species in the particle core and shell ("trapped" species concept).[22] A first set of lipid nanoparticles loaded with a hydrophobic cyanine dye (DiD) has previously been developed in our group,[21] and their *in vivo* potentialities for tumor targeting following their intravenous injection demonstrated in mice.[23] In the present study, modified formulations with human-use approved ingredients are loaded with different organic dyes whose absorption/emission spectra span from the visible to the near-infrared spectrum. We focus on a detailed exploration of the optical

---

Address all correspondence to: Isabelle Texier, LETI DTBS, CEA, 17 rue des martyrs, Grenoble, 38054 France; Tel: +33 438 784 670; Fax: +33 438 785 787; E-mail: isabelle.texier-nogues@cea.fr.

1083-3668/2011/16(9)/096013/10/$25.00 © 2011 SPIE

properties of these new contrast agents, termed as “lipidots.” Their long-term colloidal and photochemical stabilities in water, their fluorescence quantum yield and brightness, as well as their photobleaching rate are quantitatively compared to those of previously described dye-loaded nanocarriers and commercial PEGylated QDs (QTracker®705 from Invitrogen). Comparison is made between lipidots and QTracker®705 concerning *in vitro* cytotoxicity on a fibroblast cell line and performance for multichannel *in vivo* imaging of lymph nodes in mice.

2 Materials and Methods

2.1 *Materials*

ICG is a kind gift from Serb Laboratories. Suppocire NC^{TM} is purchased from Gattefossé (Saint-Priest, France). Myrj^{TM} 52, polyethylene glycol 40 stearate, and Super Reffined Soybean Oil are from Croda Uniqema (Chocques, France). QTracker®705, DiO, DiI, DiD, and DiR dyes (Fig. 1) are purchased from Invitrogen. The organic dyes are purified by column chromatography on silica gel, using cyclohexane/ethyl acetate gradient for elution, before use. Lipoid S75 (soybean lecithin at >75% phosphatidylcholine) is purchased from Lipoid (Germany), and other chemical products are purchased from Sigma Aldrich (Saint-Quentin Fallavier, France).

2.2 *Lipidot Preparation*

80 μl of a 10 mM dye solution in CH_2Cl_2 (EtOH for ICG) are poured in a 5 ml vial. The solvent is then evaporated under vacuum before an oil premix is added. The amount of oil, Suppocire NC^{TM}, and lecithin used in the oil premix are, respectively, 25, 75, and 150 mg for formulation of 30 nm diameter lipidots (F30), 85, 255, and 65 mg for 50 nm (F50), 102, 308, and 50 mg for 80 nm (F80), 144, 431, and 50 mg for 100 nm (F100), and 150, 450, and 45 mg for 120 nm (F120). After homogeneization at 60°C, the continuous aqueous phase, composed of 350 mg of Myrj^{TM} 52 for F30, 345 mg for F50, 300 mg for F80, 325 mg for F100, 215 mg for F120, and of the appropriate amount of aqueous medium (154 mM NaCl if not stated otherwise, qsp 2 ml), is introduced. The vial is placed in a 60°C water bath and the mixture is sonicated for 5 min using a VCX750 ultrasonic processor (power output 190 W, 3-mm probe diameter, Sonics). Lipidots are dialyzed overnight at room temperature against 1000 times their volume in the appropriate aqueous buffer (12–14,000 Da MW cut off membranes, ZelluTrans). Finally, the lipidot dispersion is filtered through a 0.22 μm Millipore membrane for sterilization before characterization and/or injection.

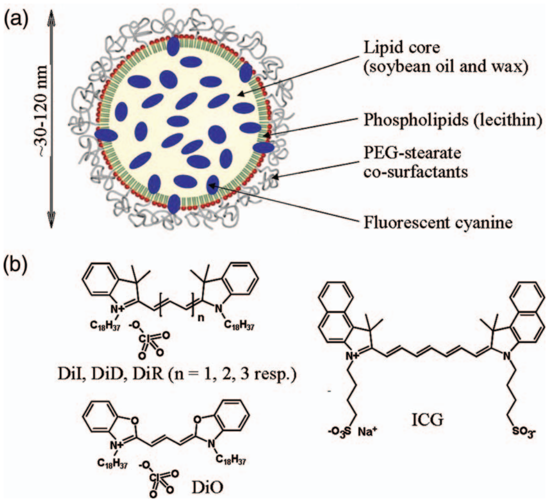

Fig. 1 Lipidot structure. (a) Lipidots are dye-loaded oily droplets dispersed in aqueous buffer, whose diameter can be adjusted between 30 and 120 nm. Their fluorescent properties are conferred by lipophilic or amphiphilic cyanine dyes (b), encapsulated in the lipid core and/or the surfactant layer.

2.3 *Size and Zeta Potential Measurements*

Dynamic light scattering is used to determine the particle hydrodynamic diameter and zeta potential (Zeta Sizer Nano ZS, Malvern Instrument). All lipidots are diluted to 2 mg/ml of lipids in sterile PBS 0.1X and are transferred in Zeta Sizer Nano cells (Malvern Instrument) before each measurement, performed in triplicate.

2.4 *Optical Properties*

The absorbance and fluorescence measurements are performed in 1X PBS, respectively, using a Cary 300 Scan UV-Visible spectrophotometer (Varian) and a Perkin Elmer LS50B fluorimeter. Previous to calculations, scattering contribution is subtracted from the absorbance spectrum using the equation:

$$D(\lambda) = \frac{a}{\lambda} + \frac{b}{\lambda^4} + c, \tag{1}$$

where a and b are fitting variables associated with Mie and Rayleigh scattering, respectively, and c is the offset at 900 nm. Fluorescence quantum yields are calculated using fluorescence standards.[24]

2.5 *Photobleaching*

Fluorescence intensities of capillaries (Ringcaps, Herschmann, internal diameter 450 μm) containing DiD-lipidots (equivalent 17 μM of DiD), 17 μM of Cy5 or 1.3 μM QT705 in water are recorded using a homemade system adapted from the commercially available Aequoria^{TM} system from Hamamatsu. The excitation device is composed of 10 light-emitting diode (LED) emitting at 633 nm (adapted from the LuxiFlux^{TM} device available from Hamamatsu). It also includes an interference bandpass filter (470DF20 from Schott) for a light illumination power of 200 μW/cm^2. The filtered fluorescence signal (filter OG515, from Schott) is measured by a cooled CCD camera (Lumen*era*), placed at 160 mm from the imaging field, with 30 ms exposure time. The LuCam Capture® software is used to drive the setup and for image processing. Fluorescence intensities are measured from the recorded images using the ImageJ® software.

2.6 *Animal Experiments*

All animal procedures are in compliance with the guidelines of the European Union (regulation n°86/609), taken in the French law (decree 87/848) regulating animal experimentation. All efforts are made to minimize animal suffering and to reduce the number of animals used. All animal manipulations are performed with sterile techniques and are approved by the Rhône-Alpes Animal Care and Use Committee (France).

2.7 *In Vivo Imaging*

Two Nude mice (Charles River, France) receive a 10 μl intradermic injection of nanoparticles (46 dyes/particle) in each paw, resulting in doses of 4 pmol of DiO-lipidots (184 pmols of dyes), 2 pmol of DiI-lipidots (92 pmol of dyes), and 1 pmol of DiD-lipidots and ICG-lipidots (46 pmol of dyes), respectively, in the front left, front right, rear left, and rear right extremity. For DiD-lipidot/QTracker®705 comparison, two Nude mice receive a 10 μl intradermic injection of 2 pmol of DiD-lipidots and 20 pmol of QTracker®705, respectively, in the rear left and rear right extremity. *In vivo* images are recorded on an IVIS® system (Xenogen) and monitored using LivingImage® software. Mice are scanned using 10 excitation (435, 465, 500, 535, 575, 605, 640, 675, 710, and 745 nm) and four emission filters, respectively, centered on the emission wavelengths of DiO, DiI, DiD, and ICG. For each emission filter, three-components spectral unmixing is carried out using the images acquired at the different excitation wavelengths (two-components for the GFP filter).

2.8 *Culture of NIH-3T3 Murine Fibroblasts*

In accordance with the International Organization for Standardization 10993, NIH-3T3 murine fibroblast cells are chosen to perform classical WST-1 cytotoxic assay. The cell line is purchased from the American Type Culture Collection. Experimental cultures are prepared from deep-frozen stock vials, and maintained in a sub-confluent state in culture Petri dish (113 cm^2) under a humidified (90%) atmosphere of 95% air/5% CO_2 at 37 °C. Cells are grown in Dulbecco's modified Eagle's medium high glucose (Gibco) supplemented with 10% newborn calf serum (PAN Biotech Gmb) and 1% antibiotics (penicillin and streptomycin) (Gibco). Culture medium is changed every other day.

2.9 *Cell Viability Assay*

Cells (5×10^4 cells/ well) are seeded in 6-well plates (Nunc). After 24 h incubation at 37°C, different concentrations of nanoparticles (DiD-lipidots or QTracker®705), from 1 to 75 nM, are added for 24 h to the culture medium followed by two washes. Each group has triplicate wells. Cytotoxicity is assessed 24 h following the nanoparticle treatment using WST-1 assay, analog to MTT assay. WST-1 reagent (Roche) is added (10%) to the culture medium and kept in the incubator for 4 h. Cells without nanoparticles and incubated with a solution of H_2O_2 10 mM are used as negative and positive controls, respectively. Absorbance is then recorded at 450 nm (soluble formazan titration) and 690 nm (background substraction) using a microplate reader (Tecan). The absorbance difference (450 to 690 nm) is directly proportional to the number of viable cells.

2.10 *Statistical Analysis*

Cell viability is expressed as a percent of viable cells calculated from the negative control. Data are compared among groups by one-way analysis of variance followed by Fisher's protected Least Significance Differences test.

3 Results

3.1 *Design and Colloïdal Properties of Dye-Loaded Lipid Nanoparticles (Lipidots)*

Complex mixtures of soluble and insoluble species, both in the lipid core [soybean oil (25% w/w) and Suppocire NC^{TM} wax (75% w/w)] and the surfactant shell [soybean lecithin (phospholipids) and PEG-based co-surfactants (Myrj^{TM} 52)] are used for lipidot design, using high-energy process to reach sub-100 nm diameter.[22,25] As previously described,[22] the heterogeneity of the lipids and surfactants mixtures constituting the nanodroplet favors its colloidal stability. In this study, typical results are presented using 50 nm diameter lipidots, but other nanoparticle sizes can easily be achieved modulating the surfactant to lipid ratio.[22,25]

Different lipophilic (Di family, log $P > 10$, P: octanol/water partition coefficient) or amphiphilic (ICG, only near-infrared dye approved for human use until now, log $P = 2.1$) cyanine dyes can be loaded in the oily phase, before addition of the aqueous phase and particle processing by ultrasonication (Fig. 1). Lipidots were then purified using dialysis, eliminating any nonencapsulated dyes and surfactants. Dye loading efficiency was calculated comparing the dispersion absorbance and fluorescence before and after dialysis. The results for 50 nm lipid nanoparticles loaded with a local dye concentration of $\approx$ 1.2 mM are displayed in Table 1. All 4 highly lipophilic indocyanines (DiO, DiI, DiD, and DiR) display encapsulation efficiency above 90% (respectively, 93%, 96%, 95%, and 92%). A lower loading value is obtained for ICG (around 77%, final local concentration of 0.9 mM), probably due to the presence of sulfonate moieties rendering this fluorophore much more hydrophilic. The approximate number of fluorescent molecules per 50-nm diameter lipidot is estimated as 44 for hydrophobic cyanines, and 36 for ICG.

Normalized emission and absorbance spectra of the different dye-loaded 50 nm diameter particles are displayed in Fig. 2. These spectra are similar to those obtained in organic solvent (CH_2Cl_2 for hydrophobic indocyanines, dimethyl sulfoxide for ICG) with a bathochromic shift inferior to 5 nm. Detailed spectral data are displayed in Table 1. The versatility of these formulations allows the production of nanoparticles with different sizes, by controlling the mass ratio of core lipids and surfactants.[22,25] Whatever the nanoparticle size, dye loading has no influence on the hydrodynamic diameter, size distribution, or zeta potential (Figs. 3 and 4). Similarly, the particle size has no effect on absorption and emission spectra of the dyes.

3.2 *Lipidots Long-Term Stability*

Colloidal stability of lipidot dispersions in 154 mM NaCl is assessed by the control of the particle hydrodynamic size, polydispersity index, and zeta potential over time. The nanoparticle diameter seems to slightly increase over time during 4°C storage: approximately 7 nm after 6 months [Fig. 4(a)]. Zeta potential does not vary significantly during this period, remaining close to neutrality [$0 < \xi < 10$ mV, Fig. 4(b)]. Coalescence

Table 1 Physicochemical characterization of 50 nm diameter lipidots.

	Dye encapsulation		Particle properties		Optical properties				
Loaded dye	Loading efficiency[a]	1 year dye stability[b]	HD (nm)[c]	ZP (mV)[d]	Abs. (nm)[e]	Em. (nm)[e]	ε (L mol^{-1} cm^{-1})[e]	Φ[e,f]	$\varepsilon \times n \times \Phi$ (L mol^{-1} cm^{-1})[e,f]
DiO	93%	48%	48 ± 3	−6.0 ± 1.5	489	505	9.0×10^4	0.39 ± 0.02	1.5×10^6
DiI	96%	93%	53 ± 3	−6.1 ± 1.6	550	567	1.2×10^5	0.31 ± 0.02	1.6×10^6
DiD	95%	52%	50 ± 3	−6.8 ± 0.6	646	668	1.3×10^5	0.53 ± 0.01	2.9×10^6
DiR	92%	NA	50 ± 1	−6.2 ± 0.8	750	775	7.0×10^4	0.21 ± 0.02	6.2×10^5
ICG	77%	89%	50 ± 3	−7.7 ± 0.6	801	820	2.0×10^5	0.06 ± 0.01	4.3×10^5
QT®705	-	-	30 ± 3	−0.7 ± 2.0	-	705	1.0×10^6	0.12 ± 0.02	1.2×10^5

[a] Results for loading ratio of 0.8 μmol of dye in 50 nm diameter particles.

[b] Percent of dyes remaining loaded in the particles with intact optical properties after 1 year storage at 4°C in dark.

[c] Hydrodynamic diameter. Standard deviation for three different measures performed in 0.1X PBS buffer (1 mM phosphate, 13.7 mM NaCl, pH 7.3).

[d] Zeta potential. Standard deviation for three different measures carried out in 0.1 X PBS buffer.

[e] Absorption maximum (Abs.), emission maximum (Em.), extinction coefficient (ε), fluorescence quantum yield (Φ), and brightness ($\varepsilon \times n \times \Phi$, n = number of dyes per particle). Measures performed in 154 mM NaCl.

[f] Excitation at 450 nm for DiO, 520 nm for DiI, 600 nm for DiD, 670 nm for DiR, 740 nm for ICG, and 590 nm for QTracker®705.

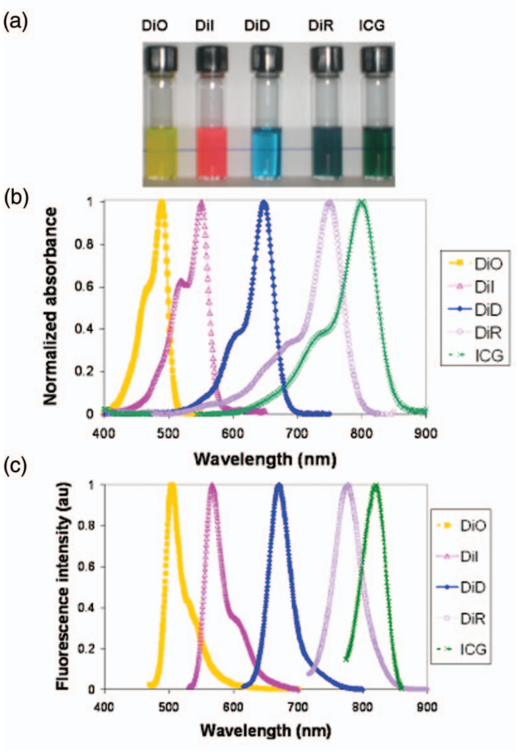

Fig. 2 Absorption (b) and emission (c) spectra of 50 nm lipidots (a) absorbing/emitting in the visible and near-infrared range. Measures performed in 154 mM NaCl aqueous solution, using lipidots loaded with 42 dyes /particle.

and Ostwald ripening are the two nanoemulsion destabilization processes. Particle coalescence is prevented by the important droplet PEG coating.[22] PEG neutral coating is also a key feature known to prevent *in vivo* opsonization of blood-circulating nanocarriers.[26–28] The use of complex mixtures for core and shell composition, as well as the suspension monodispersity, limit Ostwald ripening.[22]

Chemical and loading stability of the fluorophores in the lipidots is assessed by performing another dialysis of the formulations after 1 year storage in 154 mm NaCl at 4°C, in dark (Table 1). DiI and ICG (despite its amphiphilic character) loaded particles display very good stability, since ≈ 90% of the dyes are still encapsulated while DiO and DiD seem to partly leak outside the particles (≈ 50% loss).

Figure 5 compares the fluorescence quantum yields of encapsulated Di dyes to their commercial hydrophilic counterparts (Cy dyes, supplier data). We observe that Di-lipidot fluorescence quantum yields are 1.6 to 3.2 times higher than those of their hydrophilic counterparts (Fig. 5, Table 1). Optical properties of ICG in aqueous solution, at concentration below 200 μm to prevent dimer formation,[29] and ICG-lipidot dispersions can be directly compared. ICG-lipidot fluorescence quantum yield is low (0.06), but this value is still a great improvement in comparison to those observed for the free dye in aqueous solution (0.003 in water and 0.01 in whole blood).[29]

Even though molar extinction coefficients of the encapsulated dyes are generally lower than those encountered in organic solvents (Table 1), the high dye local concentration per nanoparticle and important fluorescent quantum yields result in

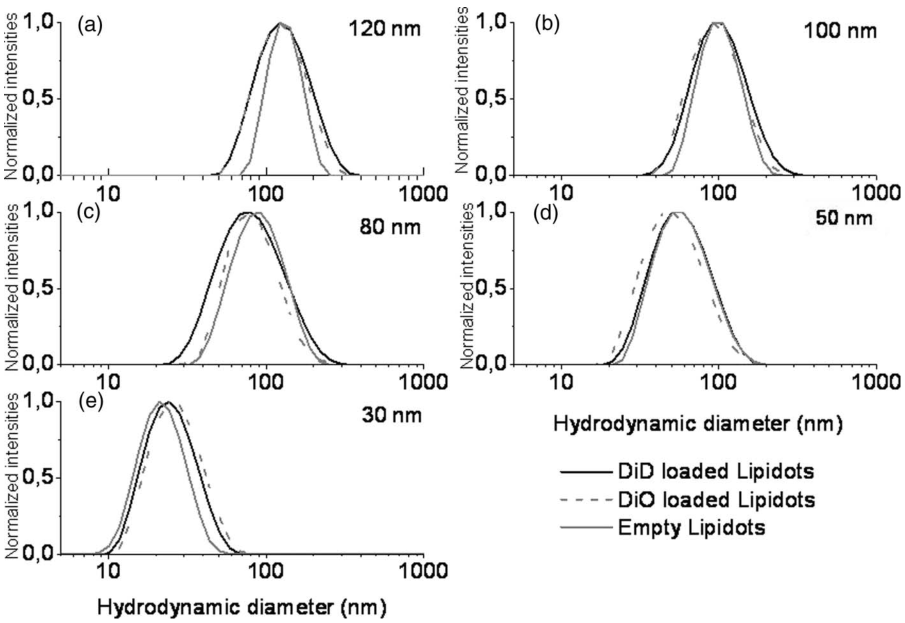

Fig. 3 Size distribution of different DiO- and DiD-lipidot formulations [mean hydrodynamic diameters: 120 (a), 100 (b), 80 (c), 50 (d), and 25 (e) nm, 1.2 mM local dye concentration].

highly bright objects. Brightness, which reflects both the fluorophore light absorption and emission abilities, well describes the quality of the optical properties of a fluorescent probe. Calculated brightness for the different lipidots loaded with ≈ 40 dyes/particle are displayed in Table 1. Furthermore, by increasing internal dye concentrations, brightness score up to 1.6 × 10^7 M^{-1} cm^{-1} has been achieved with DiD-loaded lipidots containing ∼350 dyes per particle [Fig. 6(b)]. Such high brightness can be achieved thanks to the limited dye self-quenching observed when increasing the fluorophore payload [Fig. 6(a)].

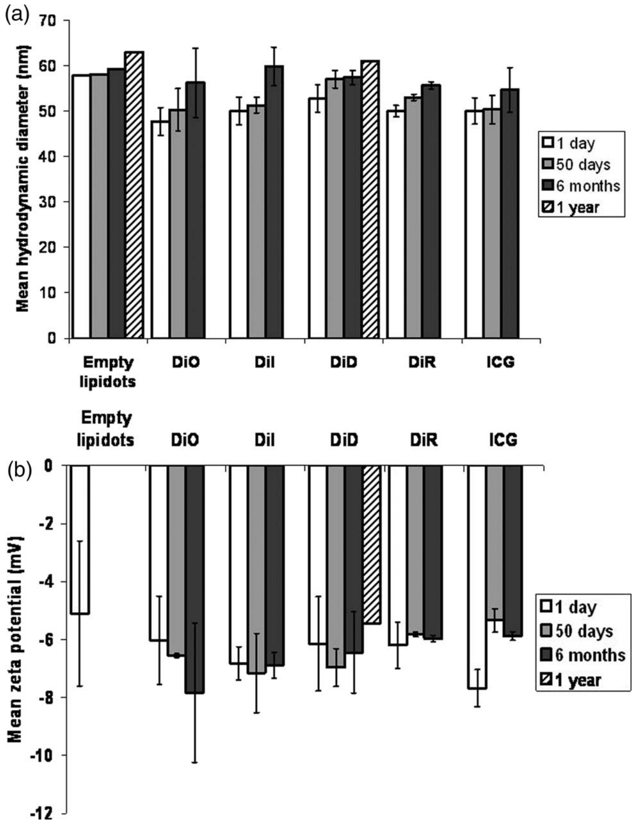

Fig. 4 Mean hydrodynamic diameter (a) and zeta potential (b) of empty and dye-loaded lipidots measured in 0.1X PBS (50 nm dispersions, 1.2 mM local dye concentration).

Figure 7 presents the photobleaching rates in water of different DiD-loaded lipidots, along with those of Cy5 and QTracker® 705, displaying emission properties in the same wavelength range. Photobleaching rates of DiD-loaded particles are slightly higher than that of Cy5. DiD-lipidots photobleaching rate is about 10 times higher than for QTracker®705.

3.3 *In Vivo Imaging with Lipidots*

The potential of lipidots for *in vivo* multichannel fluorescence imaging is explored by injecting "standard" (i.e., 46 dyes/particle) DiO-lipidots (4 pmol particles), DiI-lipidots (2 pmol particles), DiD-lipidots (1 pmol particles), and ICG-lipidots (1 pmol particles) intradermally in the paws of Nude

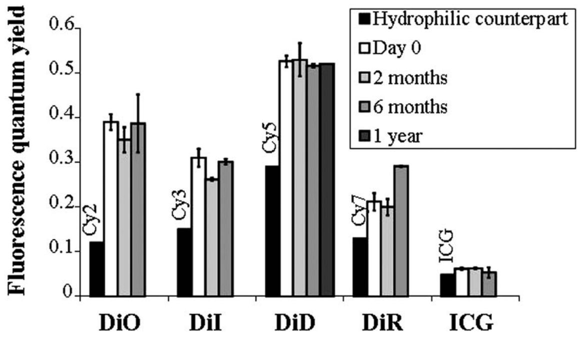

Fig. 5 Lipidot fluorescence quantum yields in 154 mM NaCl just after formulation and at different time points during storage at 4°C in dark.

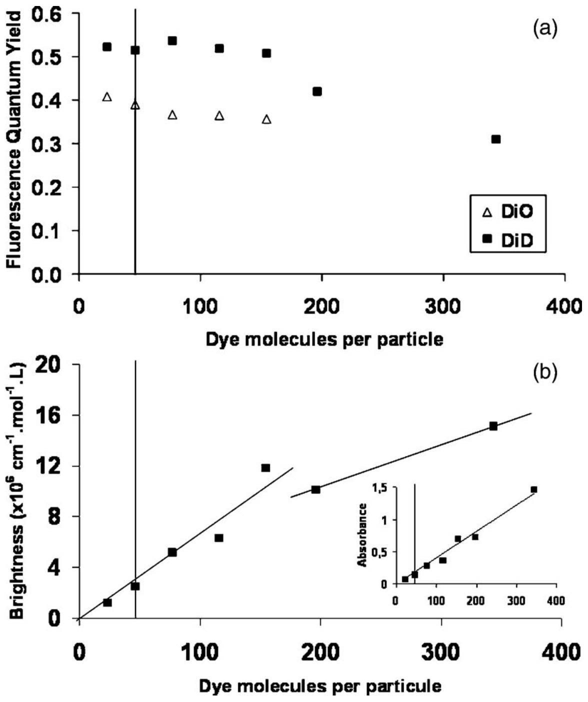

Fig. 6 Influence of dye-loading ratio on 50 nm lipidot emission properties. Standard formulations with 1.2 mM local dye concentration are indicated with a vertical solid line. (a) Fluorescence quantum yields of DiD- (black squares) and DiO- (white triangles) loaded nanoparticles. (b) Calculated brightness of DiD-loaded lipidots. Inset: absorbance for 30 nm particle dispersions.

mice. Minimal cross-talk between the different channels is observed. Fluorescence signal shows that nanoparticles are mainly restricted to the paw surface area, indicating that lipidots remain relatively confined to the interstitial space after intradermal injection. This can promote their progressive drainage through lymphatic system. When injection sites are masked with black tape, migration and accumulation of the DiD- and ICG-loaded lipidots in lymph nodes is evidenced [Fig. 8(a)]. Popliteal, then caudal lymph nodes, and eventually liver, become and remain fluorescent up to a few weeks with DiD [Fig. 8(b)], while ICG fluorescence has disappeared 24 h post-injection [Fig. 8(c)]. As expected, no signal is observed with the more blueshifted fluorophores (DiO, DiI) despite higher injection doses (2 to 4 pmol), further demonstrating the importance of near-infrared wavelengths for *in vivo* experiments.[30]

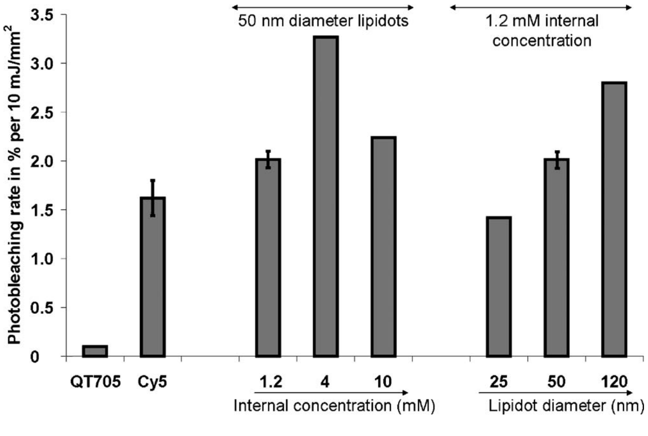

Fig. 7 Photobleaching rates of Qtracker®705, Cy5, 50 nm lipidots loaded with increasing local concentrations of DiD (corresponding to 46, 150, or 350 DiD molecules per particle), and DiD-loaded lipidots with increasing diameters (respectively 7, 46, and 557 dyes per particle for an equivalent local dye concentration of 1.2 mM).

Based on these results, lymph node imaging using DiD-loaded lipidots or QTracker™705 is then compared. Figure 9 shows that injection of 10 times less lipidots (2 pmol particles) than QTracker®705 (20 pmol particles) leads to a comparable lymph node fluorescence signal. Both DiD and QTracker®705 signals tend to last over a long period of time (up to 5 weeks).

3.4 *In Vitro Cytotoxicity Assessment*

In vitro cytotoxicity of lipidots is compared to that of QTracker®705 on NIH-3T3 cell line (mouse fibroblast) both through a WST-1 assay [Fig. 10(a)] and microscopy [Fig. 10(b)]. Even for the highest concentration of DiD-loaded nanoparticles investigated (75 nM), there is still 70% of cell viability 24 h after incubation. On the contrary, IC_{50} is reached between 25 and 35 nM for QTracker®705, with cell viability of approximately 15% when the particle concentration reaches 35 nM. Moreover, microscopy evidences that cytotoxicity occurs through different mechanisms: lipid nanoparticles modify the cell morphology and their adhesion to the plastic walls is hindered, while QDs induce cell destruction, with much cell debris visible on the images.

4 Discussion

In this study, we demonstrate that lipidots display long-term colloidal, chemical, and photochemical stabilities, high brightness in buffered media, and reduced cytotoxicity. Their wide range of size and wavelength emissions allows their use in numerous applications: while shorter wavelengths would be suitable for *in vitro* or *ex vivo* studies, NIR emitting lipidots can be used for sensitive multichannel imaging in mice. Other dye-loaded carriers such as silica,[31,32] calcium-phosphate[33–35] or polymeric nanoparticles,[36–40] micelles,[41] dendrimers,[42] liposomes,[43] lipoproteins,[44] and viruses[44,45] have also been described. For all these nanoparticles, dye encapsulation in inorganic or organic matrixes has benefits on fluorophore solubility and chemical stability in water. However, most of these carriers display either low dye loading efficiency,[46] important dye leakage,[40] low colloidal stability,[41] complicated or solvent-based manufacturing process,[34,36–38] cytotoxicity,[31,32] or could induce inflammation.[47–50] Herein, we demonstrate that 50 nm sized lipid nanoparticles loaded with NIR dyes (DiD, ICG) have suitable diameter, low cytotoxicity, and optical properties suited for efficient lymph node imaging in mice models.

As fluorescence contrast agents, lipidots are easy to produce, composed of generally recognized as safe and bio-assimilable ingredients, display high brightness over a wide range of wavelengths, and show long term storage stability. In the literature, such long-term stability is generally achieved by using specific conservation techniques such as freeze-drying after addition of cryoprotectants,[51–53] whereas no specific conservation procedure is applied here. For *in vivo* applications, small neutral particles, below 100 nm, are preferred in order to improve *in vivo*

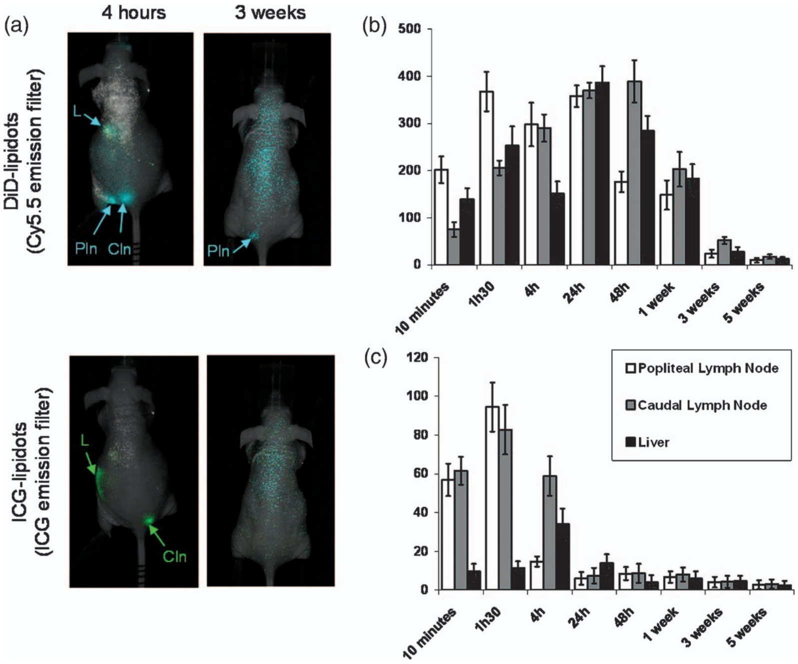

Fig. 8 Lymph node detection on Ivis® system after spectral unmixing (L: liver, Cln: caudal lymph node, Pln: popliteal lymph node). (a) DiD-lipidots (pseudo-colored blue) and ICG-lipidots (pseudo-colored green) are injected, respectively, in the left rear and right rear paws of the same animal, and are easily differentiated from autofluorescence background (white). Probably due to release from the core of the nanoparticles while metabolization, the dyes display very different kinetic behaviors: DiD emission in the lymph nodes (b) reaches its maximum intensity in ≈24 to 48 h and is cleared much more slowly than the ICG signal (c). (Color online only.)

stealth.[54] Moreover, nanocarriers can be sterilized using microfiltration, a process easier to implement than thermal or x-ray treatments, known for destabilizing lipid nanoparticles.[55,56]

The oily core of these new nanoparticles allows the encapsulation of a wide variety of hydrophobic molecules. Commercially available Di indocyanines with long alkyl chains, usually devoted to membrane labeling, are efficiently loaded resulting in the production of highly bright nanoparticles. ICG, though more hydrophilic, is also encapsulated with 77% efficiency. Lipidots stability over 1 year appears to be only hindered by the chemical sensitivity of the dyes. This is especially shown in the case of DiR (emission wavelength 775 nm) which degrades in a matter of weeks when stored in PBS. Near-infrared emitting indotricarbocyanines are known for their polyethylene backbone fragility.[57] Cleavage of the polyethylene chain, for instance in the presence of oxidizing species, typically leads to shorter

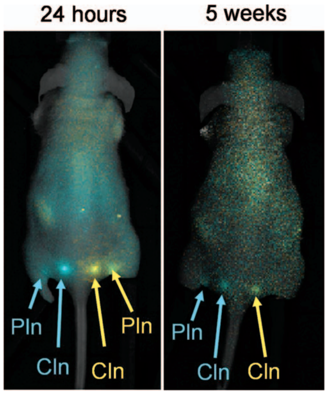

Fig. 9 Lymph node detection on Ivis® system after spectral unmixing (Cy5.5 emission filter). 2 pmol of DiD-lipidots (pseudo-colored blue) and 20 pmol of QTtracker® 705 (pseudo-colored yellow) are injected intradermally, respectively, in the rear left and rear right paw of the mice (L: liver, Cln: caudal lymph node, Pln: popliteal lymph node). (Color online only.)

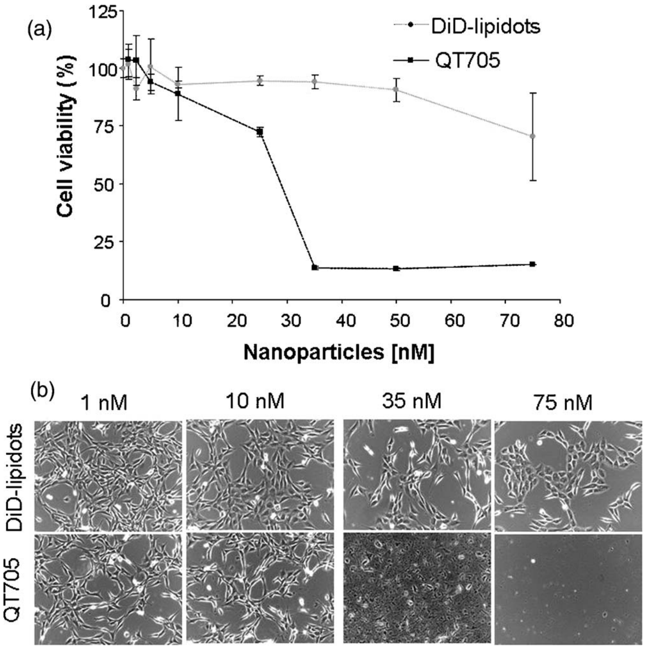

Fig. 10 Cell viability (WST-1 assay after a 24 h contact, (a) and microscopy imaging (b) of NIH-3T3 fibroblasts incubated in the presence of increasing concentrations of 50 nm diameter DiD-lipidots or QTracker® 705.

conjugated products, known to absorb in the 450 to 650 nm range, as observed here for DiR dispersions. After a year, ICG and DiI encapsulations are shown to be very stable while DiD and DiO partially escape from the particle core. Given the structural proximity between all the dyes, this difference between aged samples suggest chemical modifications of DiD and DiO, altering their hydrophilic/hydrophobic balance, rather than an intraparticular solubility issue.

Brightness scores of lipidots range from 4×10^5 to 3×10^6 $\mathrm{L\,cm^{-1}\,mol^{-1}}$ in "standard" formulations (≈ 40 dyes/particle) and higher results are achieved when the number of dyes per particle is increased (up to 13×10^6 $\mathrm{L\,cm^{-1}\,mol^{-1}}$ with 350 DiD molecules per particle). To the best of our knowledge, these brightnesses are comparable to the highest values reported in the literature for QDs (up to 4×10^6 $\mathrm{M^{-1}\,cm^{-1}}$),[58] dye-loaded silica nanoparticles (up to $\sim 2 \times 10^6$ $\mathrm{M^{-1}\,cm^{-1}}$),[59] or polymeric micelles (up to 5×10^5 $\mathrm{M^{-1}\,cm^{-1}}$),[37] although these objects display smaller particle sizes (≈15 nm). Photobleaching of lipidots is comparable to what is observed with Cy5, depending on their size and loading: bleaching rate raises by 63% when the internal dye concentration reaches 4 mm, then goes back to normal at 10 mm. A possible explanation for this is that with increasing concentration, photoproduced radicals are more likely to react with a neighboring fluorophore. When internal concentration reaches the self-quenching value [above 4 mm, 200 dyes/particle, Fig. 6(a)] photoproduction of radicals is reduced. However, for an equivalent particle concentration, 10 mm DiD-loaded lipidots are 18 times brighter than QTracker®705. This means that dye-concentrated lipidots can undergo a substantial photobleaching and yet still display a significant fluorescence signal. Moreover, all the photobleaching rates displayed in Fig. 7 remain very low (2% to 3% for an hour of continuous illumination) in comparison to the time necessary for small animal imaging (1 min/point).

Lipidots present the strong advantage to be colloidally stable and have the optimized size range (~50 nm) reported in the literature for lymph node retention.[14,20] Lipid-based nanocarriers display affinity for lymphatic channels and lymph nodes.[20] Perfluorocarbon-oil–based nanoemulsions encapsulating lipophilic dyes were shown to be efficient lymph node contrast agents for fluorescence or photoacoustic imaging.[17] Due to their 220-nm diameter, they displayed slower diffusion through the lymphatic channels and improved node retention in comparison to the free dyes.[17] Interestingly, the impact of particle size was also studied using gold particles (4-nm diameter) encapsulated in polymeric (290-nm diameter) or lipid (90-nm diameter) nanovectors.[18] Whereas 290 nm particles displayed very poor transportation in the lymphatic channels, an important photoacoustic signal could be observed traveling through the lymphatic system and then accumulating in the lymph nodes in 20 min following intradermal injection in a rat of 90 nm gold-lipid nanoparticles.[18] In the present study, dye-loaded lipid nanoparticles with smaller sizes (typically 50-nm diameter) are used. Such small sizes associated with a good colloidal stability can be achieved thanks to the formulation composition and to ultrasonic processing.[22] The presently described imaging experiments reveal that lipidots can rapidly and strongly stain lymph nodes draining the injection site with a persistent signal over time (>24 h) depending on the dye used. After ICG-lipidot injection, ICG signal displays a maximum accumulation within lymph node between 1 h 30 min and 4 h post-injection. On the contrary, DiD signal persists for long duration (up to 5 weeks). Whereas ICG is known to be excreted in 1 to 2 days by the hepato-biliary pathway,[60] hydrophobic Di cyanines, known markers of cell membranes, are retained on the long term. This quicker clearance observed for ICG could be either due to degradation and metabolization of lipidots, releasing their fluorophore content, or escape of the amphiphilic dye in the lymph. Comparison between DiD-loaded lipidots and QTracker®705 showed that lymph node were stained and displayed similar fluorescence intensities with 10 times less organic nanoparticles. The cytotoxicity experiments evidence that lipid nanoparticles are less likely to induce side-effects than cadmium-based QDs. Optimization of the dye loading should allow further reduction of the amount of injected lipidots, thus minimizing possible occurrence of side effects. Therefore, lipidots appear as promising probes for lymph node mapping in clinics.

5 Conclusion

Lipidots are able to encapsulate a wide variety of lipophilic and amphiphilic indocyanine dyes, thus displaying various emission wavelengths from 505 to 820 nm. Encapsulation within these nanoparticles is efficient and stable over 1 year, only hindered by the chemical stability of the dyes. Trapping of the indocyanines within nanoparticles enhance their optical properties, allowing to reach high brightness scores. Lipidots also prove to have suitable colloidal properties for long-term storage in an injection-ready formulation. *In vivo* experiments show that lipidots are suitable for multichannel imaging and can compete with quantum dots in lymph node detection after intradermal injection. Being composed of GRAS components, these new fluorescent contrast agent evidence reduced *in vitro* toxicity in comparison with semiconductor nanocrystals. They are also well tolerated without any inflammation induction even with high-dose intravenous injection (150 mg/kg of lipids in rats, data not shown). Easy to produce in a wide range of size and emission wavelengths, storable over a long period of time in standard conditions, highly bright and well tolerated *in vivo*, lipidots are very promising tools for fluorescence imaging and clinical applications.

Acknowledgments

We acknowledge the Molinspiration Property Calculation Service (www.molinspiration.com) for dye logP calculation and Michel Berger and Normann Mangeret for experimental support for the photobleaching experiments. This work is supported by the Commissariat à l'Energie Atomique et aux Energies Alternatives (CEA), and the French National Research Agency (ANR) through Carnot funding and in the frame of its program in Nanosciences and Nanotechnologies (CALIF project N°ANR-08-NANO-006).

References

1. S. Gross and D. Piwnica-Worms, "Molecular imaging strategies for drug discovery and development," *Curr. Opin. Chem. Biol.* **10**, 334–346 (2006).
2. J. K. Willmann, N. Van Bruggen, L. M. Dinkelborg, and S. S. Gambhir, "Molecular imaging in drug development," *Nat. Rev. Drug Discovery* **7**, 591–607 (2008).

3. E. A. te Velde, T. Veerman, V. Subramaniam, and T. Ruers, "The use of fluorescent dyes and probes in surgical oncology," *Eur. J. Surg. Oncol.* **36**, 6–15 (2010).
4. J. L. Figueiredo, C. Siegel, M. Nahrendorf, and R. Weissleder, "Intraoperative near-infrared fluorescent cholangiography (NIRFC) in mouse models of bile duct injury," *World J. Surg.* **34**, 336–343 (2010).
5. J. C. Rasmussen, I. C. Tan, M. V. Marshall, C. E. Fife, and E. M. Sevick-Muraca, "Lymphatic imaging in humans with near-infrared fluorescence," *Curr. Opin. Biotechnol.* **20**, 74–82 (2009).
6. S. L. Troyan, V. Kianzad, S. L. Gibbs-Strauss, S. Gioux, A. Matsui, R. Oketokoun, L. Ngo, A. Khamene, F. Azar, and J. V. Frangioni, "The FLARE intraoperative near-infrared fluorescence imaging system: a first-in-human clinical trial in breast cancer sentinel lymph node mapping," *Ann. Surg. Oncol.* **16**, 2943–2952 (2009).
7. I. Miyashiro, N. Miyoshi, M. Hiratsuka, K. Kishi, T. Yamada, M. Ohue, H. Ohigashi, M. Yano, O. Ishikawa, and S. Imaoka, "Detection of sentinel node in gastric cancer surgery by indocyanine green fluorescence imaging: comparison with infrared imaging," *Ann. Surg. Oncol.* **15**, 1640–1643 (2008).
8. Y. Ogasawara, H. Ikeda, M. Takahashi, K. Kawasaki, and H. Doihara, "Evaluation of breast lymphatic pathways with indocyanine green fluorescence imaging in patients with breast cancers," *World J. Surg.* **32**(9), 1924–1929 (2008).
9. N. Tagaya, R. Yamazaki, A. Nakagawa, A. Abe, K. Hamada, K. Kubota, and T. Oyama, "Intraoperative identification of sentinel lymph nodes by near-infrared fluorescence imaging in patients with breast cancer," *Am. J. Surg.* **195**(6), 850–853 (2008).
10. N. Unno, M. Suzuki, N. Yamamoto, K. Inuzuka, D. Sagara, N. Nishiyama, H. Tanaka, and H. Konno, "Indocyanine Green fluorescence angiography for intraoperative assessment of blood flow: a feasibility study," *Eur. J. Vas. Endovasc Surg.* **35**, 205–207 (2008).
11. C. Hirche, D. Murawa, Z. Mohr, S. Kneif, and M. Hünerbein, "ICG fluorescence-guided sentinel node biopsy for axilliary nodal staging in breast cancer," *Breast Cancer Res. Treat.* **121**, 373–378 (2010).
12. S. Gioux, H. S. Choi, and J. V. Frangioni, "Image-guided surgery using invisible near-infrared light: fundamentals of clinical translation," *Mol. Imaging* **9**(5), 237–255 (2010).
13. E. M. Sevick-Muraca, R. Sharma, J. C. Rasmussen, M. V. Marshall, J. A. Wendt, H. Q. Pham, E. Bonefas, J. P. Houston, L. Sampath, K. E. Adams, D. K. Blanchard, R. E. Fischer, S. B. Chiang, R. Elledge, and M. E. Mawad, "Imaging of lymph flow in breast cancer patients after microdose administration of a near-infrared fluorophore," *Radiology* **246**(3), 734–741 (2008).
14. S. Onishi, S. J. Lomnes, R. G. Laurenc, A. Gobashian, G. Mariani, and J. V. Frangioni, "Organic alternatives to quantum dots for intraoperative near-infrared fluorescent sentinel lymph node mapping," *Mol. Imaging* **4**(3), 172–181 (2005).
15. S. Kim, Y. T. Lim, E. G. Soltesz, A. M. De Grand, J. Lee, A. Nakayama, J. A. Parker, T. Mihaljevic, R. G. Laurence, D. M. Dor, L. H. Cohn, M. G. Bawendi, and J. V. Frangioni, "Near-infrared fluorescent type II quantum dots for sentinel lymph node mapping," *Nat. Biotechnol.* **22**(1), 93–97 (2004).
16. H. Kobayashi, Y. Hama, Y. Koyama, T. Barett, C. Regino, Y. Urano, and P. L. Choyke, "Simultaneous multicolor imaging of five different lymphatic basins using quantum dots," *Nano Lett.* **7**(6), 1711–1716 (2007).
17. W. J. Akers, C. Kim, M. Y. Berezin, K. Guo, R. Fuhrhop, G. M. Lanza, G. M. Fischer, E. Daltrozzo, A. Zumbusch, X. Cai, L. V. Wang, and S. Achilefu, "Noninvasive photoacoustic and fluorescence sentinel lymph node identification using dye-loaded perfluoropcarbon nanoparticles," *ACS Nano* **5**(1), 173–182 (2011).
18. D. Pan, M. Pramanik, A. Senpan, S. Ghosh, S. A. Wickline, L. V. Wang, and G. M. Lanza, "Near infrared photoacoustic detection of sentinel lymph nodes with gold nanobeacons," *Biomaterials* **31**, 4088–4093 (2010).
19. H. S. Choi, W. Liu, W. Misra, E. Tanaka, J. P. Zimmer, B. I. Ipe, M. G. Bawendi, and J. V. Frangioni, "Renal clearance of quantum dots," *Nat. Biotechnol.* **25**(10), 1165–1170 (2007).
20. Y. Nishioka and H. Yoshino, "Lymphatic targeting with nanoparticulate system," *Adv. Drug Delivery Rev.* **47**(1), 55–64 (2001).
21. I. Texier, M. Goutayer, A. Da Silva, L. Guyon, N. Djaker, V. Josserand, E. Neumann, J. Bibette, and F. Vinet, "Cyanine loaded lipid nanoparticles for improved in vivo fluorescence imaging," *J. Biomed. Opt.* **14**(5), 054005 (2009).
22. T. Delmas, H. Piraux, A. C. Couffin, I. Texier, F. Vinet, P. Poulin, M. E. Cates, and J. Bibette, "How to prepare and stabilize very small nanoemulsions," *Langmuir* **27**(5), 1683–1692 (2011).
23. M. Goutayer, S. Dufort, V. Josserand, A. Royère, E. Heinrich, F. Vinet, J. Bibette, J. L. Coll, and I. Texier, "Tumor targeting of functionalized lipid naoparticles: assessment by in vivo fluorescence imaging," *Eur. J. Pharm. Biopharm.* **75**, 137–147 (2010).
24. I. Texier and E. Heinrich, "Inhibition of fluorescent dyes for the design of efficient activatable probes dedicated to non-invasive small animal imaging," *Proc. SPIE* **6449**, 64490I (2007).
25. T. Delmas, A. C. Couffin, P. A. Bayle, F. de Crécy, E. Neumann, F. Vinet, M. Bardet, J. Bibette, and I. Texier, "Preparation and characterisation of highly stable lipid nanoparticles with amorphous core of tuneable viscosity," *J. Colloid Interf. Sci.* **360**, 471–481 (2011).
26. M. Hamidi, A. Azadi, and P. Rafiei, "Pharmacokinetic consequences of Pegylation," *Drug Deliv.* **13**, 399–409 (2006).
27. S. Tamilvanan, "Oil-in-water lipid emulsions: implications for parenteral and ocular delivering systems (review)," *Prog. Lipid Res.* **43**, 489–533 (2004).
28. V. P. Torchilin, "Multifunctional nanocarriers," *Adv. Drug Deliv. Rev.* **58**, 1532–1555 (2006).
29. R. C. Benson and H. A. Kues, "Fluorescence properties of indocyanine green as related to angiography," *Phys. Med. Biol.* **23**(1), 159–163 (1978).
30. R. Weissleder, "A clearer vision for *in vivo* imaging," *Nature Biotechnol.* **19**(4), 316–317 (2001).
31. Y.-S. Lin and C. L. Haynes, "Impacts of Mesoporous Silica Nanoparticle Size, Pore Ordering, and Pore Integrity on Hemolytic Activity," *J. Am. Chem. Soc.* **132**(13), 4834–4842 (2010).
32. D. Napierska, L. C. J. Thomassen, V. Rabolli, D. Lison, L. Gonzalez, M. Kirsch-Volders, J. A. Martens, and P. H. Hoet, "Size-Dependent Cytotoxicity of Monodisperse Silica Nanoparticles in Human Endothelial Cells," *Small* **5**(7), 846–853 (2009).
33. M. Epple, K. Ganesan, R. Heumann, J. Klesing, A. Kovtun, S. Neumann, and V. Sokolova, "Application of calcium phosphate nanoparticles in biomedicine," *J. Mater. Chem.* **20**, 18–23 (2010).
34. E. I. Altinoglu, T. J. Russin, J. M. Kaiser, B. M. Barth, P. C. Eklund, M. Kester, and J. H. Adair, "Near-infrared emitting fluorophore-doped calcium phosphate nanoparticles for in vivo imaging of human breast cancer," *ACS Nano* **2**(10), 2075–2084 (2008).
35. H. S. Muddana, T. T. Morgan, J. H. Adair, and P. J. Butler, "Photophysics of Cy-3 encapsulate calcium phosphate nanoparticles," *Nano Lett.* **9**(4), 1559–1566 (2009).
36. R. Weissleder, C.-H. Tung, U. Mahmood, and A. Bogdanov Jr., "In vivo imaging of tumors with protease activated near infrared fluorescent probes," *Nature Biotech.* **17**, 375–378 (1999).
37. G. Sun, M. Y. Berezin, J. Fan, H. Lee, J. Ma, K. Zhang, K. L. Wooley, and S. Achilefu, "Bright fluorescent nanoparticles for developing potential optical imaging contrast agents," *Nanoscale* **2**, 548–558 (2010).
38. Z. Yang, J. Leon, M. Martin, J. W. Harder, R. Zhang, D. Liang, W. Lu, M. Tian, J. G. Gelovani, A. Qiao, and C. Li, "Pharmacokinetics and biodistribution of near-infrared fluorescence polymeric nanoparticles," *Nanotechnol.* **20**, 165101 (2009).
39. P. Ghoroghchian, P. Frail, K. Susumu, D. Blessington, A. Brannan, F. Bates, B. Chance, D. Hammer, and M. Therien, "Near IR emissive polymersome: self-assembled soft matter for in vivo optical imaging," *Proc. Natl. Acad. Sci. U. S. A.* **102**(8), 2922–2927 (2004).
40. V. Saxena, M. Sadoqi, and J. Shao, "Enhanced photo-stability, thermal-stability and aqueous-stability of indocyanine green in polymeric nanoparticulate systems," *J. Photochem. Photobiol. B* **74**, 29–38 (2004).
41. A. Papagiannaros, A. Kale, T. S. Levchenko, D. Mongayt, W. C. Hartner, and V. P. Torchilin, "Near infrared planar tumor imaging and quantification using nanosized Alexa 750-labeled phospholipid micelles," *Int. J. Nanomed.* **4**(1), 123–131 (2009).
42. S. H. Medina and M. E. El-Sayed, "Dendrimers as carriers for delivery of chemotherapeutic agents," *Chem. Rev.* **109**, 3141–3157 (2009).
43. V. Deissler, R. Rüger, W. Frank, A. Fahr, W. A. Kaiser, and I. Hilger, "Fluorescent liposomes as contrast agents for in vivo optical imaging of edemas in mice," *Small* **4**(8), 1240–1246 (2008).

44. D. P. Cormode, P. A. Jarzyna, W. Mulder, and Z. A. Fayad, "Modified natural nanoparticles as contrast agents for medical imaging," *Adv. Drug Deliv. Rev.* **62**, 329–338 (2010).
45. S. A. Hilderbrand, K. Kelly, M. Niedre, and R. Weissleder, "Near infrared fluorescence-based bacteriophage particles for ratiometric pH imaging," *Bioconjugate Chem.* **19**, 1635–1639 (2008).
46. I. Miletto, A. Gilardino, P. Zamburlin, S. Dalmazzo, D. Lovisolo, G. Caputo, G. Viscardi, and G. Martra, "Highly bright and photostable cyanine dye-doped silica nanoparticles for optical imaging: Photophysical characterization and cell tests," *Dyes Pigm.* **84**, 121–127 (2010).
47. B. Fubini and A. Hubbard, "Reactive oxygen species (ROS) and reactive nitrogen species (RNS) generation by silica in inflammation and fibrosis," *Free Radic Biol. Med.* **34**(12), 1507–1516 (2003).
48. K.-T. Yong, I. Roy, M. T. Swihart, and P. Prasad, "Multifunctional nanoparticles as biocompatible targeted probes for human cancer diagnosis and therapy," *J. Mater. Chem.* **19**, 4655–4672 (2009).
49. A. Burns, H. Ow, and U. Wiesner, "Fluorescent core-shell silica nanoparticles: towards "lab on a particle" architectures for nanobiotechnology," *Chem. Soc. Rev.* **35**, 1028–1042 (2006).
50. A. Burns, J. Vider, H. Ow, E. Herz, O. Penate-Medina, M. Baumgart, S. M. Larson, U. Wiesner, and M. Bradbury, "Fluorescent silica nanoparticles with efficient urinary excretion for nanomedicine," *Nano Lett.* **9**(1), 442–448 (2009).
51. A. del Pozo-Rodriguez, M. A. Solinis, A. R. Gascon, and J. L. Pedraz, "Short- and long-term stability study of lyophilized solid lipid nanoparticles for gene therapy," *Eur. J. Pharm. Biopharm.* **71**(2), 181–189 (2009).
52. H. Ohshima, A. Miyagishima, T. Kurita, Y. Makino, Y. Iwao, T. Sonobe, and S. Itai, "Freeze-dried nifedipine-lipid nanoparticles with long-term nano-dispersion stability after reconstitution," *Int. J. Pharm.* **377**(1–2), 180–184 (2009).
53. R. K. Subedi, K. W. Kang, and H. K. Choi, "Preparation and characterization of solid lipid nanoparticles loaded with doxorubicin," *Eur. J. Pharm. Sci.* **37**(3–4), 508–513 (2009).
54. S. M. Moghimi, A. C. Hunter, and J. C. Murray, "Long-circulating and target-specific nanoparticles: theory to practice," *Pharmacol. Rev.* **53**(2), 283–318 (2001).
55. W. Mehnert and K. Mäder, "Solid lipid nanoparticles: production, characterization and applications," *Adv. Drug Deliv. Rev.* **47**, 165–196 (2001).
56. B. Heurtault, P. Saulnier, B. Pech, J.-E. Proust, and J.-P. Benoit, "Physico-chemical stability of colloidal lipid particles," *Biomaterials* **24**, 4283–4300 (2003).
57. D. Oushiki, H. Kojima, T. Terai, M. Arita, K. Hanaoka, Y. Urano, and T. Nagano, "Development and application of a near-infrared fluorescence probe for oxidative stress based on differential reactivity of linked cyanine dyes," *J. Am. Chem. Soc.* **132**(8), 2795–2801 (2010).
58. J. A. Rochira, M. V. Gudheti, T. J. Gould, R. R. Laughlin, J. L. Nadeau, and S. T. Hess, "Fluorescence Intermittency Limits Brightness in CdSe/ZnS Nanoparticles Quantified by Fluorescence Correlation Spectroscopy," *J. Phys. Chem. C* **111**(4), 1695–1708 (2007).
59. D. R. Larson, H. Ow, H. D. Vishwasrao, A. A. Heikal, U. Wiesner, and W. W. Webb, "Silica nanoparticle architecture determines radiative properties of encapsulated fluorophores," *Chem. Mater.* **20**, 2677–2684 (2008).
60. T. Desmettre, J.-M. Devoisselle, and S. Mordon, "Fluorescence properties and metabolic features of Indocyanine Green (ICG) as related to angiography," *Surv. Ophthalmol.* **45**(1), 15–27 (2000).